Received: 26 February 2021 | Revised: 2 April 2021 | Accepted: 2 May 2021

DOI: 10.1002/maco.202112385

ARTICLE

Materials and Corrosion

Bioactivity and corrosion behavior of magnesium barrier membranes

Helga Hornberger[1,2] | **Hannah Kissel**[1] | **Birgit Striegl**[2] | **Matthias Kronseder**[3] | **Florian Vollnhals**[4,5] | **Silke Christiansen**[6,7]

[1]Biomaterials Laboratory, Faculty of Mechanical Engineering, Ostbayerische Technische Hochschule (OTH), Regensburg, Germany

[2]Regensburg Center of Biomedical Engineering (RCBE), Ostbayerische Technische Hochschule (OTH) and University of Regensburg, Regensburg, Germany

[3]Institute of Experimental and Applied Physics, University of Regensburg, Regensburg, Germany

[4]Institute for Nanotechnology and Correlative Microscopy (INAM) gGmbH, Forchheim, Germany

[5]Leuchs Emeritus Group, Max Planck Institute for the Science of Light, Forchheim, Germany

[6]Department Correlative Microscopy and Materials Data, Fraunhofer Institute for Ceramic Technologies and Systems (IKTS), Forchheim, Germany

[7]Physics Department, Freie Universität Berlin (FU), Berlin, Germany

Correspondence
Helga Hornberger, Biomaterials Laboratory, Faculty of Mechanical Engineering, Ostbayerische Technische Hochschule (OTH), Galgenbergstr. 30, Regensburg 93053, Germany.
Email: helga.hornberger@oth-regensburg.de

Abstract

In the current research, magnesium and its alloys have been intensively studied as resorbable implant materials. Magnesium materials combine their good mechanical properties with bioactivity, which make them interesting for guided bone regeneration and for the application as barrier membranes. In this study, the in vitro degradation behavior of thin magnesium films was investigated in cell medium and simulated body fluid. Three methods were applied to evaluate corrosion rates: measurements of (i) the gaseous volume evolved during immersion, (ii) volume change after immersion, and (iii) polarization curves. In this comparison, measurements of H_2 development in Dulbecco's modified Eagle's medium showed to be the most appropriate method, exhibiting a corrosion rate of 0.5 mm·year^{-1}. Observed oxide and carbon contamination have a high impact on controlled degradation, suggesting that surface treatment of thin foils is necessary. The bioactivity test showed positive results; more detailed tests in this area are of interest.

KEYWORDS

bioactivity, corrosion rate, degradation, dental membrane, magnesium

1 | INTRODUCTION

The application of membranes is a standard procedure for guided bone regeneration (GBR) in the area of dental implant and periodontal surgery, and generally in facial surgery. Surgeons use artificial membranes if a new bone is meant to be rebuild. The principle is based on the insertion of a barrier membrane to separate regenerative cell types like osteoblasts, which show relatively slow proliferation, from connective tissue cells, which show

TABLE 1 Composition of magnesium foils in m/m%

Al	Cu	Fe	Mn	Ni	Si	Zn	Ca	Mg
<0.005	<0.005	0.03	<0.005	<0.005	<0.005	<0.005	<0.005	Rest

TABLE 2 Concentrations of ions and components in c-SBF and DMEM

Ion or component	Unit	c-SBF	DMEM
Na^+	mmol/L	142.0	154.5
K^+	mmol/L	5.0	5.4
Mg^{2+}	mmol/L	1.5	0.8
Ca^{2+}	mmol/L	2.5	1.8
Cl^-	mmol/L	147.8	118.5
HCO_3^-	mmol/L	4.2	44.0
HPO_4^{2-}	mmol/L	1.0	0.9
SO_4^{2-}	mmol/L	0.5	0.8
Tris	g/L	6.118	-
Amino acids	g/L	-	1.6
Glucose	g/L	-	4.5

Abbreviations: c-SBF, corrected simulated body fluid; DMEM, Dulbecco's modified Eagle's medium.

typically rapid proliferation. In this way, membranes enable a predictable and guided regeneration of a lost or missing bone tissue by protecting a cavity. The first generation of membranes was made of nonresorbable materials such as expanded polytetrafluoroethylene (e-PTFE), cellulose acetate, and titanium. Those membranes have been widely used due to their ability of long-term cavity maintenance, demonstrating successful GBR treatment in many cases.[1] Titanium membranes in the form of porous meshes have the advantage of a better supply of blood and nutrition.[2] The second generation are resorbable membranes made of collagen, primarily of porcine or bovine origin.[2] Barrier membranes are indicated for only temporary use until the bone regeneration or augmentation is completed. This means that inert membranes made of e-PTFE or titanium have to be removed in a second surgical intervention. This carries a risk of infection and/or tissue damage; the latter is not unlikely in the case of delicate and thin facial tissue structures. Therefore, resorbable collagen membranes will be mainly applied in the dental and craniomaxillofacial surgery. Compared with titanium meshes, however, collagen membranes show relatively low mechanical strength and less ability for cavity preservation. However, although both resorbable and nonresorbable membranes appear to promote bone coverage of the initial surface, nonresorbable membranes were susceptible to higher complication rates in vivo.[3]

Requirements for resorbable GBR barrier membranes include biocompatibility and bioactivity, cavity preservation, and ease of handling for the surgeons. Bioactivity in the case of GBR means the ability of osseointegration to promote bone growth on the implant surface. Furthermore, appropriate stiffness for space maintenance, the ability to prevent epithelial cell migration, and a tailored degradation time after bone regeneration is completed are the specific requirements to achieve maximum bone regeneration. Magnesium foils allow for new applications in oral and facial surgery as degradable membranes due to high mechanical stability combined with resorbability. However, the degradation process of many magnesium materials still carries the risk of inhomogeneous corrosion. This means that very fast corrosion rates, combined with the formation of gas bubbles and strong pH increase, are locally possible. A strong pH increase may damage cells and tissue. The formation of gas bubbles may separate the tissue, and such a separation will take time to disappear and can cause pain for the patient.

Although many corrosion studies of magnesium materials in electrolytes similar to body liquids have been carried out, for example, Refs. [4–21], this study brings into focus the in vitro degradation behavior of thin magnesium foil samples with a greater relation of surface area to their volume. Using pH-controlled fluids similar to body liquid as electrolytes, extensive insight into the applied corrosion test methods will be included to contribute to the scientific effort to establish reliable in vitro test methods similar to in vivo conditions and to allow other labs to reproduce tests easily. Besides the determination of corrosion rates, the surfaces will be characterized to get a deeper insight into degradation and bioactivity behavior.

2 | EXPERIMENTAL METHODS

2.1 | Immersion corrosion tests

Magnesium foils (99.9% [m/m] Mg; Goodfellow) having a diameter of 8 mm and a thickness of 0.1 mm (volume of

5.0 mm^3) were used to allegorize dental membranes. The composition according to the manufacturer is shown in Table 1. Immersion tests and electrochemical tests were carried out in Dulbecco's modified Eagle's medium (DMEM) (SH30585-02; Merck) and in corrected simulated body fluid (c-SBF) according to Kokubo and Takadama[22] to study the degradation behavior of the magnesium foils. The compositions of the applied electrolytes are shown in Table 2. Working with cell medium, approximately sterile conditions were applied in every step. Before testing, each sample was ultrasonically cleaned for 10 min in isopropanol. During the immersion tests in c-SBF and in DMEM, the temperature control of the incubator (ICO150med; Memmert) was set to 37.7 ± 0.3°C to achieve the temperature of 37.4°C within the electrolytes. The relation of electrolyte volume (EV) to sample surface area (SA) was set to EV:SA = 225 $ml{\cdot}cm^{-2}$ for both systems. Kirkland et al.[4] recommended EV:SA > 50 $ml{\cdot}cm^{-2}$, because smaller ratios affect the corrosion rate.[4] The ratio was the same in all corrosion tests to secure the comparison of data. Furthermore, every 24 h, the electrolyte was renewed by taking a new test setup and changing rapidly the sample from one to the other setup.

The pH of DMEM solution during corrosion test was regulated using CO_2/HCO_3^- buffering system. For this, CO_2 gas was added during the immersion periods into the atmosphere of the incubator chamber (Figure 1). The pH of DMEM was monitored and kept at 7.4 by adding constantly 7.3% CO_2 into the chamber. The pH of the c-SBF solution was buffered with Tris to 7.4 and also monitored during tests. The experimental setup of the immersive corrosion tests (Figure 1) was based on the classical setup of Song et al.[23] Cell sieves with pore sizes of 100 μm were used to carry the foils; as a result, the entire surface of the foils was in contact with the electrolyte. The evolving gas was measured in regular intervals. However, before a 24-h immersion test with renewed electrolyte was started, the electrolyte and test setup were preheated for 2 h in the incubator without magnesium foil. It was observed that some gas already evolved without immersed magnesium sample. This can be attributed to the decreased solubility of dissolved gases in the electrolyte and the increase of water vapor during the increase in temperature. This gas evolution was marked first before starting the corrosion test. Then the gas volume (V_{meas}) evolved during corrosion of magnesium could be measured from the difference of the markers (Figure 1).

To calculate the corrosion at a pH of 7.4, it was assumed that the following reactions take place at the interface of magnesium and electrolyte:

$$\text{Anodic reaction: } Mg \rightarrow Mg^{2+} + 2e^-, \quad (1)$$

$$\text{Cathodic reaction: } 2H_2O + 2e^- \rightarrow 2OH^- + H_2. \quad (2)$$

In this way, the mol amount (n) of corroded magnesium is equivalent to the mol amount of evolved hydrogen. It needs the application of the ideal gas equation and the norm volume (V_0) of H_2 to calculate the amount of mol H_2:

$$n = \frac{V_0 \times p_0}{R \times T_0}, \quad (3)$$

where $p_0 = 101{,}325$ Pa, $T_0 = 273.15$ K, and R = ideal gas constant.

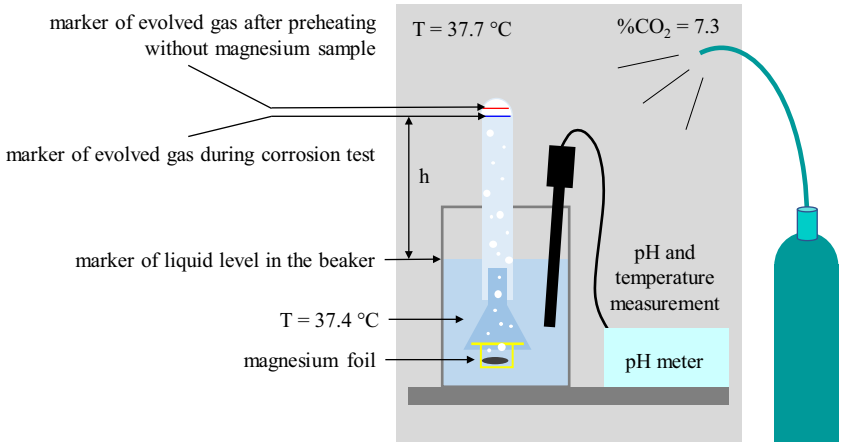

FIGURE 1 Schematic depiction of Dulbecco's modified Eagle's medium immersion test setting measuring the H_2 evaluation. First, the test setup was preheated for 2 h without sample to release the dissolved gases (red marker). Then, the corrosion test was started. The evolved gas volume due to the corrosion process was measured by the difference between the two markers (red and blue) [Color figure can be viewed at wileyonlinelibrary.com]

The normal volume V_0 was calculated with the following equation:

$$V_0 = \frac{p_{H_2} \times V_{H_2} \times T_0}{p_0 \times T_{test}}, \quad (4)$$

where $V_{H_2} = V_{meas}$ = gas volume evolved during immersion test and $T_{test} = 300.15$ K (temperature during immersion test).

The partial pressure of H_2 (p_{H_2}) was determined by the following approach:

$$p_{H_2} = \rho_e \times g \times h + p_{atm} - p_{vapor}, \quad (5)$$

where h = measured height (see Figure 1), $\rho_e = 0.99333$ g·cm^{-3} (density of the electrolyte at $T = T_{test}$), $g = 9.81$ m·s^{-2}, p_{atm} = atmospheric local pressure at the testing dates, and $p_{vapor} = 6265$ Pa (saturated vapor pressure at T_{test}).

The partial pressure of evolving gases other than H_2 and water vapor during the immersion time was neglected. Therefore, there might have been less hydrogen gas evolved than considered in calculation. On the other side, the solubility of H_2 in the electrolyte was also neglected. This means that the initially evolved hydrogen is taken by the electrolyte until saturation, and it does not escape as gas bubbles. In this way, the measured gas may reflect less than the entire amount of H_2 molecules, which have developed during the immersion test.

Using Equation (3), the amount of mol (n) for each measurement was calculated, and from this, the volume and mass loss (W) of the corroding magnesium were determined:

$$\text{Mass loss } (W_m) = n \times M_{Mg}, \quad (6)$$

$$\text{Volume loss } (W_v) = \frac{n \times M_{Mg}}{\rho}, \quad (7)$$

where $M_{Mg} = 24.305$ g·mol^{-1} (molecular mass of magnesium) and $\rho = 1.738$ g·cm^{-3} (density of magnesium).

Finally, the rate of corrosion (CR) in mm·year^{-1} could be calculated according to ASTM G31:

$$CR = \frac{W_m}{A \times \rho \times t}, \quad (8)$$

where $A = 1$ cm^2 (magnesium foil surface exposed to corrosion) and t = period of immersion.

2.2 | Microcomputed tomography (micro-CT)

Magnesium foils before and after immersion were studied using micro-CT. For this, the immersed samples were first carefully rinsed in distilled water and then dried in the incubator before micro-CT investigation. All scans were performed on the system phoenix v|tome|x s 240/180 research edition from Waygate Technologies Digital Solutions Baker Hughes. Scanning parameters were as follows: 50−55 kV voltage, 450–750 μA current, 1000-ms time, 3000 images, and voxel size 12 μm. Reconstructed volumes were processed using software phoenix datos|x 2 reconstruction 2.4.0. Three-dimensional (3D) images and surface area and volume parameters were determined using software Volume Graphics VG Studio Max 3.1. The threshold value defining the material and background was set to 0.10 absorption coefficient. Volumes and surfaces were determined before and after the immersion test. Volumes according to higher and lower absorption coefficients were evaluated after immersion to correct the volume loss for calculation of CR:

$$CR = \frac{V}{A \times t}, \quad (9)$$

where ΔV = the loss of Mg volume after immersion and A = evaluated surface area.

2.3 | Electrochemical studies

For electrochemical studies of three magnesium foils, the mini-cell system (Ibendorf), the potentiostat PGSTAT204, and Software Nova 2.1 (Metrohm) were used. The measurements were performed at room temperature with the electrolytes DMEM and c-SBF. To facilitate electron conduction, three foils were glued with silver conductive epoxy adhesive to aluminum plates. A scan rate of 10 mV·s^{-1} was used to measure a polarization curve; this fast scan is possible by application of the mini-cell system.[24] Polarization resistance R_p was determined at the corrosion potential $E_{corr} \pm 30$ mV. For the calculation of the current corrosion density i_{corr}, the Tafel constants were assumed to be 0.12 V·dec^{-1}. The CRs were then calculated according to ASTM G102:

$$CR = K \times \frac{M \times i_{corr}}{\rho \times z}, \quad (10)$$

where $z = 2$ assuming Equation (1) and K = the factor to convert in unit mm·year^{-1}.

2.4 | Bioactivity studies

The immersion tests were performed according to a previous study[22] to evaluate the bioactivity behavior of magnesium foils. The c-SBF composition is shown in Table 2, and the pH was adjusted to 7.4. The EV:SA ratio

was set to 100 ml·cm^{-2} for all bioactivity tests. After preheating the electrolyte, the sample was placed vertically into the vessel. Samples were immersed for 2 and 28 days. The electrolyte was changed when the pH increased to pH ≥7.5.

Long-term tests, ideally some weeks, are necessary to study bioactivity because the formation of hydroxyapatite may need up to 4 weeks. It was observed that the thin foils degraded too strongly during this time needed and could not be considered for 28-day immersion tests. Therefore, cylinders were cut from magnesium rods (99.96% [m/m]) with a diameter of 10 mm and a height of 10 mm, and then embedded in epoxy, grinded, and polished to achieve a defined surface.

2.5 | Additional characterization studies

2.5.1 | Scanning electron microscopy (SEM)

To study the magnesium foil surface before immersion, SEM images were acquired using a Zeiss Auriga FE-SEM at 3 kV acceleration voltage using an ET-type detector for secondary electron detection. The system is equipped with an EDX system (80 mm^2) from Oxford Instruments. Energy-dispersive X-ray spectroscopy (EDX) data were collected at 3 keV beam energy using the INCA software package. The helium ion beam of a Zeiss Orion Nanofab Helium Ion Microscope (HIM) was used to acquire secondary electron images at an energy of 30 keV and a beam current of 0.2 pA. The cross-section of corroded foil samples after immersion in DMEM was studied using SEM Leo 1455 VP at 4-kV acceleration voltage.

2.5.2 | X-ray photoelectron spectroscopy (XPS)

Surface layer composition before and after the immersion tests was qualitatively determined by XPS PHI 5700 XPS/ESCA. In addition, the surfaces were sputtered with an argon ion beam of 1.5 kV for 30 min to remove some of the surface impurities.

2.5.3 | X-ray diffraction (XRD)

For phase analysis of the grown Ca-phosphate surface layer after bioactivity test, XRD measurements were performed at Fraunhofer Institute for Silicate Research (FHG ISC), Wuerzburg (Germany), using PANalytical Empyrean S2 (Malvern Panalytical). Thereby, survey scans of samples before and after immersion in c-SBF were performed. Furthermore, measurements with a constant gracing incidence at 0.5°, 1.0°, and 1.5° were carried out to increase the interaction with thin surface layers.

3 | RESULTS

3.1 | Study of magnesium foil surfaces

In slow-operating SEM scans of Mg foils before immersion tests, many large charging spots on the surface could be detected. A corresponding EDX mapping study revealed a correlation between the high concentration of oxygen and the bright spots in the SEM picture (Figure 2, left). This translates into an inhomogeneous oxide distribution. Hence, spots with high oxide concentration cause an insulating effect during electron microscopy. Using HIM, the artifacts appear dark and suggest that there are regions that contain oxide and carbon, whereas the bright areas contain probably only very thin oxide layers (Figure 2, right). In both microscopes, a nonhomogeneous surface composition was observed on the micrometer scale.

XPS has an information depth of at most 10 nm. The spectra directly after inserting foils from ambient conditions are mainly composed of carbon and oxygen (24%–57%) from the atmospheric environment (Figure 3). After a soft surface treatment by Ar ion sputtering, the spectral composition changes in the sense that the carbon peak strongly decreases, the magnesium peak intensity increases, and the oxygen concentration settles between 41 and 56 (Figure 3). In Figure 3, the remainder to reach 100% corresponds to the oxygen content.

3.2 | H_2 evolution during immersion tests

Seven Mg foils were immersed in DMEM and two in c-SBF for various periods. Figure 4a demonstrates the decreasing volume of magnesium calculated by the observed gas evolution, depending upon the immersion time. The volume loss in c-SBF was much higher than in DMEM. The volume decrease in DMEM appears to have a lower gradient, whereas the SBF shows corrosion attack that is more aggressive in the initial period. The higher corrosion attack found in c-SBF is probably caused by the higher amount of chloride ions as compared with DMEM (Table 2). Chloride ions are known to have a significant impact on the increase of corrosion rate.[6,25]

Calculation of degradation rates reflects also the high initial attack of c-SBF as compared with the initial attack in DMEM (Figure 4b). In both electrolyte systems, the

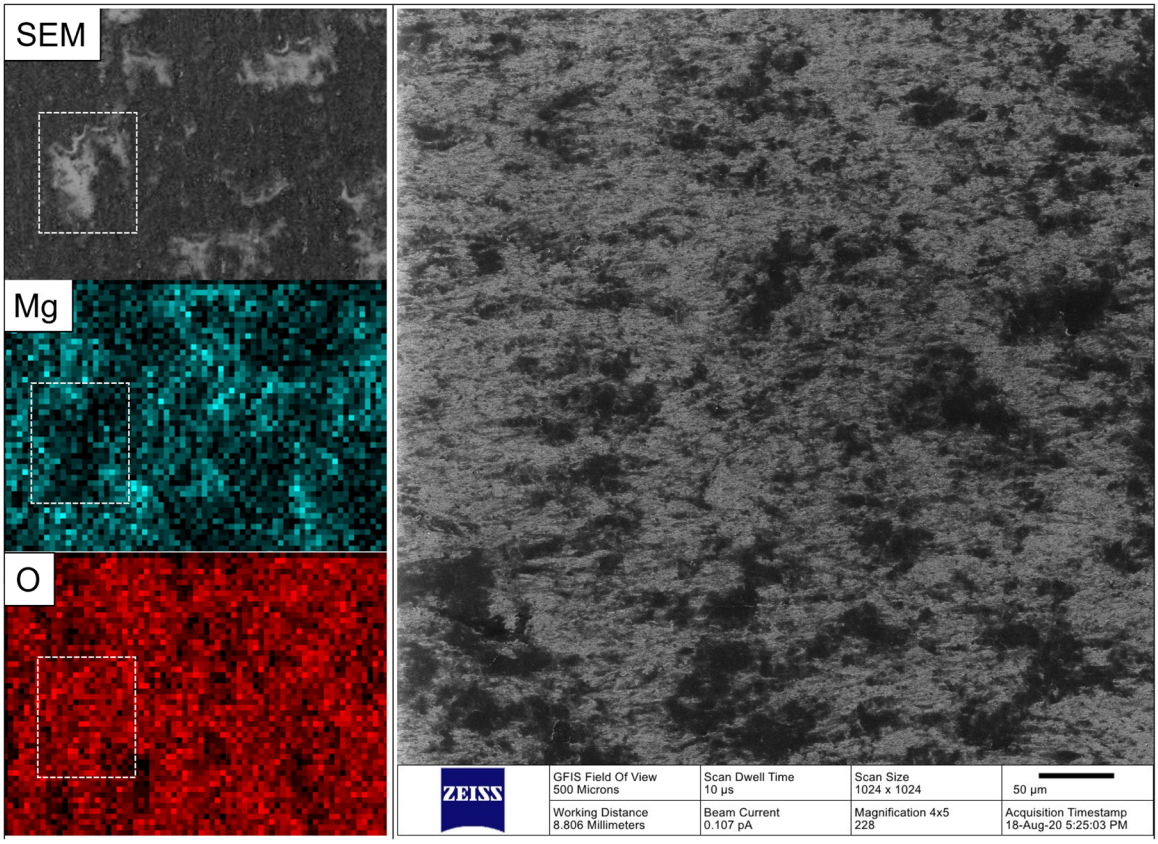

FIGURE 2 Left: scanning electron micrsoscopy (SEM) picture of the foil before immersion test and energy-dispersive X-ray spectroscopy mapping of magnesium and oxygen at the same place. Bright spots in the SEM picture correlate thereby with low magnesium and high oxygen concentrations. Field of view: 125 × 100 µm. Right: helium ion microscope picture shows the inhomogeneous surface of foils before immersion test. The dark areas correlate with thicker oxide layers than bright areas [Color figure can be viewed at wileyonlinelibrary.com]

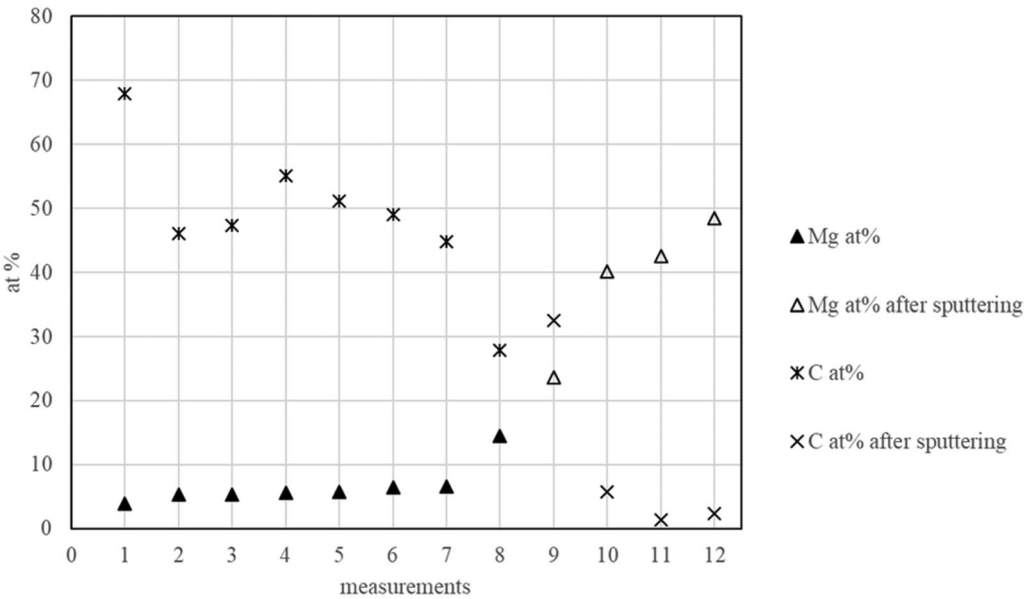

FIGURE 3 X-ray photoelectron spectroscopy analyses before immersion tests show a low magnesium content and a high carbon content. After sputtering of 30 min, the concentration of magnesium increases

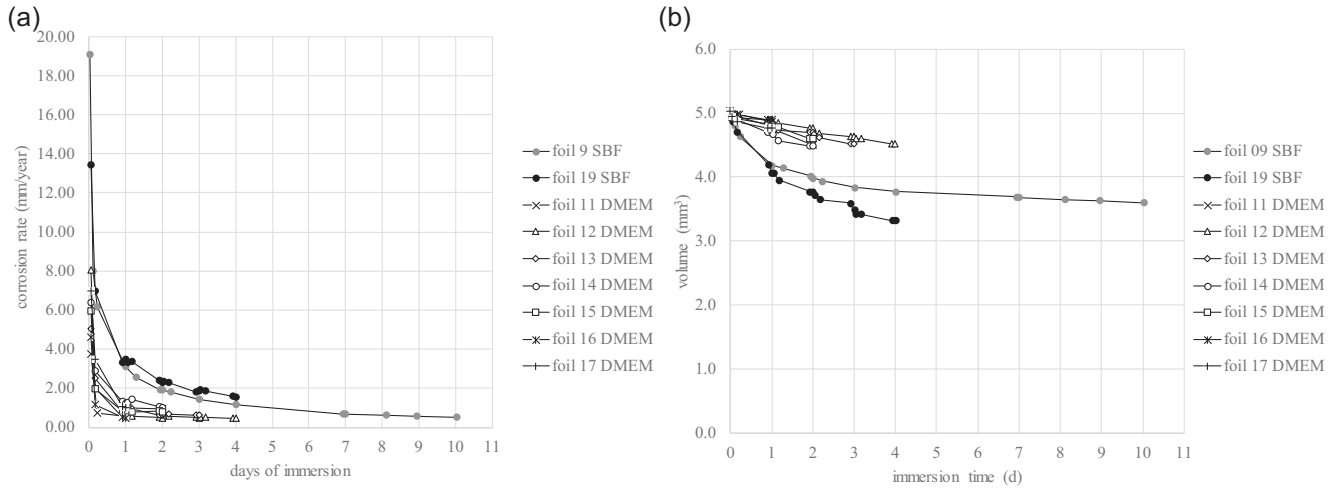

FIGURE 4 Calculations from H_2 data. (a) Decreasing foil volume during immersion corrosion tests in Dulbecco's modified Eagle's medium (DMEM) and simulated body fluid (SBF). (b) Mg foils show a decreasing corrosion rate over time of immersion; thereby SBF produces higher corrosion rates and furthermore, the approach of constant corrosion rates appears faster in DMEM than in SBF

corrosion rate is approaching a value of about 0.5 mm·year^{-1} with increasing time, respectively, after 4 days in DMEM and after 10 days in c-SBF. This means the approach of constant corrosion rates appears faster in DMEM than in SBF. Generally, the decrease of CR was also found in other studies.[7,8,25,26] Alkalization of the electrolyte during immersion can be a reason for decreasing CR, but this can be excluded, as the pH of the electrolyte was constant during experiments. It appears that a partially protective layer built up during immersion is responsible for reduced corrosion rates. Typically, a very high degradation rate can be found at the beginning, which then decreases and finally becomes constant.

Comparison with a degradation study of Mg–0.3Ca alloy in DMEM showed a similar behavior.[8] However, the CR appeared lower than in the present Mg foil study. In the present study, magnesium foils showed at the beginning a CR in DMEM of about 4–8 mm·year^{-1}, compared with 0.6 mm·year^{-1}, and in long term of about 0.5 mm·year^{-1}, compared with 0.2 mm·year^{-1}.[8] Reasons for the higher corrosion rates might be the composition of the magnesium foils, the composition of the DMEM used, and the microstructure. The magnesium foils have a purity of 99.9% (m/m), which means that the impurity levels are higher than the tolerance levels and accelerated corrosion rates can be expected.[9,26] Compared with the study of Nidadavolu et al.,[8] the 10% fetal bovine serum was not supplemented to DMEM electrolyte, and thus a higher corrosion rate can be expected because those proteins reduce the reaction and corrosion rates.[27] Finally, microstructural features like grain size have an effect on corrosion rate.[14,28] However, the grain sizes and the typical grain shape within the foil bulk were not determined in this study. Furthermore, this information is also often missing in other studies, and therefore comparisons are limited.

Figure 4b demonstrates the decreasing corrosion rates, considering that the reason for the decrease of the corrosion rates over time is oxidic corrosion products, which have already built up in DMEM after 4 days but not in c-SBF. However, during immersion tests in c-SBF, protective corrosion products can obviously form after 10 days to slow down corrosion.

3.3 | Micro-CT study after immersion tests

Six foils tested in DMEM and one tested in c-SBF were analyzed via micro-CT before and after immersion. Figure 5 (upper level) shows the reconstructed 3D data of some foils before and after immersion tests, and it demonstrates the more aggressive as well as different attacks in c-SBF as compared with degradation in DMEM. The geometry of the foils has only slightly changed after DMEM immersion. On the contrary, the disc shape has changed in a rapid and significant way after degradation in c-SBF. As the 3D reconstructions of samples immersed in DMEM do not show a significant change after immersion, the CT volume data of those foils were analyzed in more detail. Two approaches demonstrate the volume decrease over immersion time, first by measuring the entire volume and second by correcting this volume due to the setting of other absorption coefficients. Figure 5 (lower level) shows that the decrease of the corrected volume data is slightly stronger than that of the entire volume. Calculations of the corrosion rate in DMEM from the corrected data show a mean value of 0.5 mm·year^{-1}. This value is in accordance with H_2 data; however, the variation of CR was found to be very high

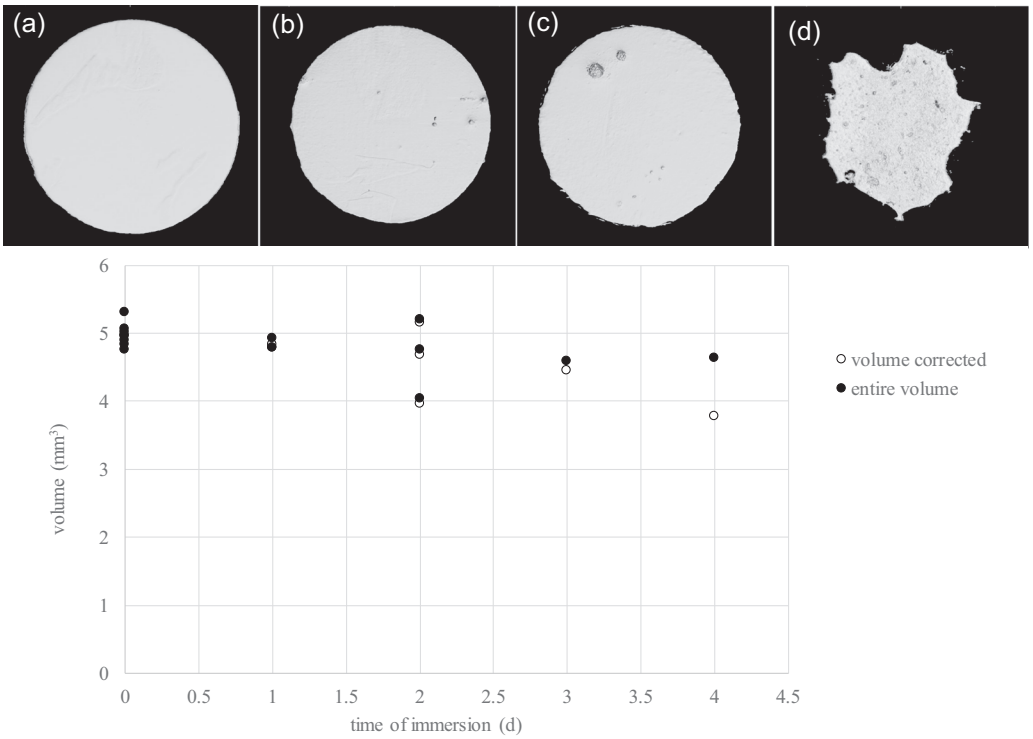

FIGURE 5 Micro-computed tomography (mico-CT) data. Upper level: The depiction of the 3D reconstruction of CT data shows foils having a diameter of (a) 7.9 mm before immersion, (b) 7.8 mm after 1-day immersion time in Dulbecco's modified Eagle's medium (DMEM), (c) 7.8 mm after 4-day immersion time in DMEM, and (d) about 6 mm after 4-day immersion time in corrected simulated body fluid. Lower level: Volume before and after immersion in DMEM shows a decrease with immersion time

(about 50%), and furthermore, the data showed no decreasing tendency with immersion time. A closer look at the absorption data showed the difficulty to distinguish between the volume of metallic magnesium and oxide phases. Therefore, the arising oxides during immersion could mostly not be detected.

The volume CT data evaluated after 4 days of immersion in c-SBF are also in accordance with H_2 data. It appeared after 4 days that less corrosion products formed on the surface in comparison with DMEM and furthermore, due to the difference in corrosion products, corrosion products might have been easier to distinguish in micro-CT. The calculated CR was 1.6 mm·year^{-1}, and no data were available for 10-day samples to compare with H_2 data.

3.4 | Electrochemical results

Polarization curves were measured on three foils, and on each foil, three measurements in DMEM and three measurements in SBF were performed. Figure 6 presents the resulting curves of one foil as an example; the other two foils showed similar behavior. Table 3 summarizes all electrochemical data and shows the strong influence of the electrolyte on the corrosion data. The magnesium foils in DMEM have higher corrosion potential E_{corr}, higher polarization resistance R_p, higher breakdown potential E_b, and lower corrosion current density i_{corr} (and thus lower corrosion rate CR) than in SBF. Corrosion potential and current density in SBF were found to be similar to other studies in SBF.[10]

The evaluated corrosion rates of 0.6 mm·year^{-1} in DMEM and 1.5 mm·year^{-1} in c-SBF are similar to the ones found by micro-CT and H_2 evaluation after 4-day immersion tests. That means that the build up of a protective oxide layer in DMEM takes place very quickly, therefore some protection is given even during polarization. On the contrary, the build up of a protective layer in SBF occurs in long term and cannot be captured by polarization measurement.

3.5 | Degradation products

3.5.1 | Immersion in DMEM

After immersion for 3 days, cross-sections of the sample foil 13 were studied using SEM. Figure 7 shows the grown conversion layer, which reveals various thicknesses between 0 and 20 μm. By assuming a uniform degradation, the calculation from H_2 volume loss data of sample foil 13 results in

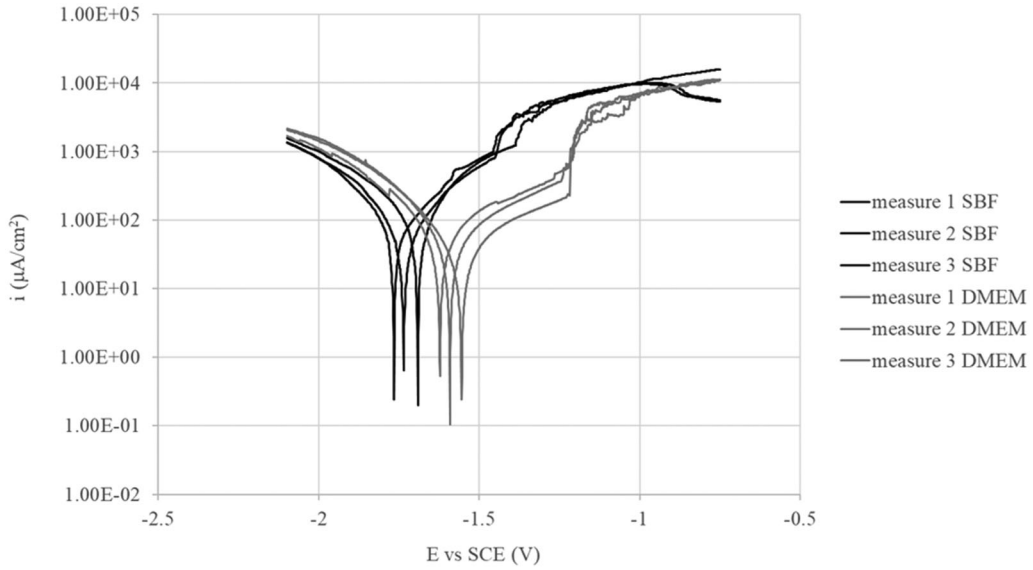

FIGURE 6 Polarization curves measured from one magnesium foil in different electrolytes; gray, Dulbecco's modified Eagle's medium (DMEM); black, corrected simulated body fluid (c-SBF)

TABLE 3 Data calculated from polarization curves

	DMEM	SBF
E_{corr} (V) versus SCE	-1.61 ± 0.05	-1.74 ± 0.03
R_p ($\Omega \cdot cm^2$)	$16{,}761 \pm 6255$	6649 ± 1558
i_{corr} ($\mu A \cdot cm^{-2}$)	26.61 ± 7.43	65.31 ± 20.68
Range of E_b (V) versus SCE	Between -1.4 and -1.2	Between -1.5 and -1.3
CR ($mm \cdot year^{-1}$)	0.61 ± 0.17	1.49 ± 0.47

Abbreviations: c-SBF, corrected simulated body fluid; CR, corrosion rate; DMEM, Dulbecco's modified Eagle's medium; SCE, saturated calomel electrode.

an effective thickness of corrosion product layer of 5 µm. Although the converted layer thickness in Figure 7 does not appear to be homogeneous, comparison with the calculated value shows the same range of order. The composition of those corrosion products was discussed in other studies; the main degradation product in DMEM appears to be magnesium carbonate[11,29] beside magnesium oxide and hydroxide.[30] Using secondary electron mode (Figure 7), the contrast of the magnesium foil is lighter than of the corrosion product layer. However, due to charging effects, the contrast of the degradation layer turns mostly white. This confirms the oxide character of the corrosion products.

3.5.2 | Immersion in c-SBF

Two types of immersion tests in c-SBF have to be differentiated: first, corrosion tests to compare the corrosion behavior in c-SBF and in DMEM, and second, bioactivity tests according to Kokubo and Takadama.[22] The latter imply to place the surface of interest vertically. The test according to Kokubo and Takadama[22] is supposed to predict the bioactivity of a sample in vivo from the formation of hydroxyapatite on its surface during in vitro immersion in SBF within 4 weeks.

In the first step, magnesium foils were soaked for 1 and for 2 days in c-SBF to study corrosion; the test setup was similar to Figure 1. After immersion, surface modification by a powdery, partially white substance deposited on the surface was observed. Possible products are again magnesium oxide, hydroxide, and carbonate, and furthermore, calcium carbonate as well as phosphates of magnesium and calcium.[12,13] XPS studies showed the presence of Ca and P on surfaces both after 1 and after 2 days of immersion in c-SBF, and no Ca and P before immersion; as an example, the XPS spectrum after 1 day of immersion is presented in Figure 8 (upper level). Thereby the Ca:P relationship increased from about 0.96 after 1 day of immersion to about 1.67 after 2 days of immersion. The latter correlates to the relation of the stoichiometric composition of hydroxyapatite.

The magnesium foils did not survive long test periods of 28 days under the aggressive conditions of c-SBF. Therefore, in the second step, instead of magnesium foils, some thick magnesium cylinders were inserted vertically for long-term bioactivity tests. XPS spectra of those samples after immersion for 2 days and for 28 days were performed. The spectra revealed the same peak positions (Ca and P) as observed on the foil samples shown in Figure 8 upper level.

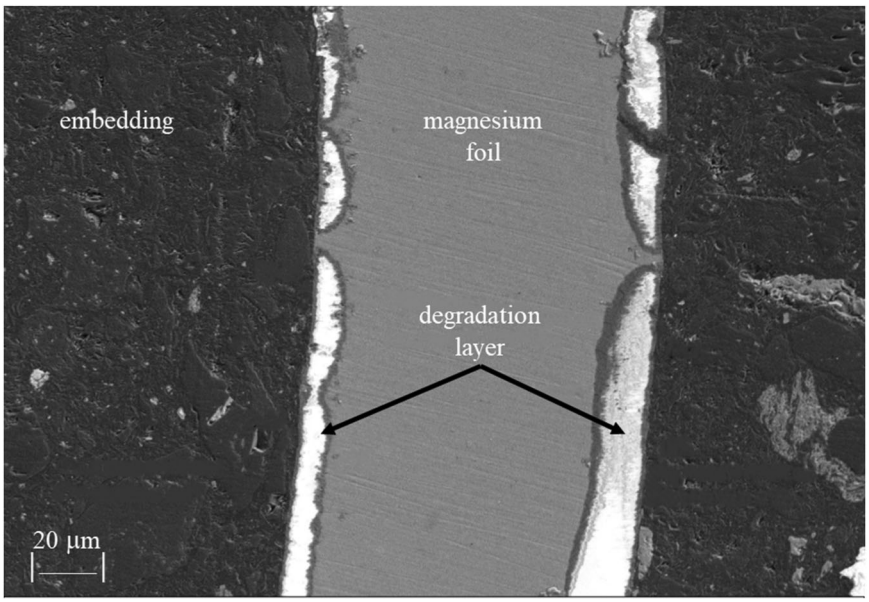

FIGURE 7 Scanning electron microscopy picture of Mg foil cross-section after immersion in Dulbecco's modified Eagle's medium for 3 days shows various thicknesses of degradation. Using secondary electron mode, the contrast of the embedding materials appears very dark and the contrast of the Mg foil appears very light. The contrast of the degradation layer appears mostly white due to the charging effects of the corrosion products

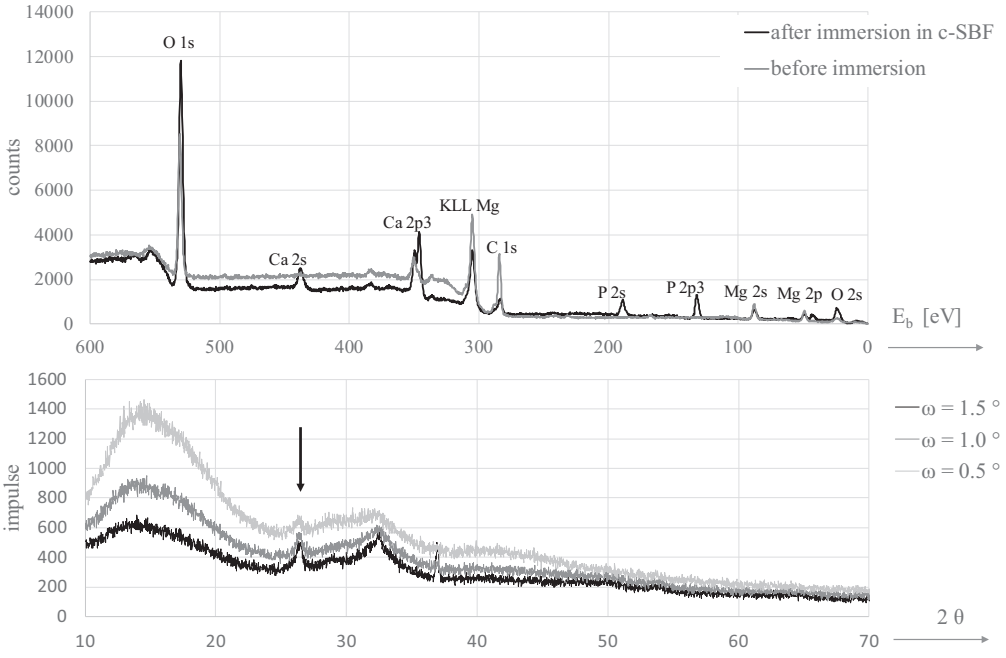

FIGURE 8 Study of the degradation layer after immersion test in corrected simulated body fluid (c-SBF). Upper level: X-ray photoelectron spectrum of a magnesium foil after 1-day immersion test in c-SBF shows Ca and P peaks. Lower level: X-ray diffraction spectrum of the surface after 28-day immersion test in c-SBF reveals a new diffraction line on the surface at 26.29°. In addition, increasing incidence angles indicate an increasing intensity of this line (marked by arrow)

However, the intensities differed, intensities measured on cylinder samples after soaking for 28 days increased, compared with those measured on foil and cylinder surfaces, which were immersed for only two days. The grown layers were additionally studied by XRD to indicate the formation of apatite. The XRD study included the surfaces of three magnesium cylinder samples: (i) before immersion test, (ii) after immersion in c-SBF for 2 days, and (iii) after immersion in c-SBF for 28 days. First, a survey of the X-ray scans was performed, which revealed clearly that in comparison to the pure magnesium substrate, an additional crystalline phase had not yet formed after 2 days but after

TABLE 4 Approached corrosion rates of magnesium foils

	DMEM	c-SBF
Immersion and H_2 evolution	0.5 mm·year^{-1}	0.5 mm·year^{-1}
Immersion and CT analysis	0.5 mm·year^{-1}	–
Electrochemical results	0.6 mm·year^{-1}	1.5 mm·year^{-1}

Abbreviations: c-SBF, corrected simulated body fluid; CT, computed tomography; DMEM, Dulbecco's modified Eagle's medium; –, not sufficient data available.

28 days, indicated by a peak at 26.29°. An XRD scan using very flat angles resulted in more details of the crystalline character of this surface layer, as shown in Figure 8 (lower level). The diffraction line at 26.29° thereby indicated increasing intensity with the increasing incidence angle. This means that the outer surface of the layer has more character that is amorphous, whereas the layer between the outer layer and magnesium substrate shows a crystalline structure.

4 | DISCUSSION

4.1 | Corrosion rates

The determination of corrosion rates is challenging for thin magnesium foils, considering nonuniform and pitting corrosion.[31] In this study, the loss of magnesium volume and mass was evaluated using three different methods: (A) measuring the amount of evolving H_2 gas during immersion, (B) measuring the change in volume by micro-CT before and after immersion, and (C) determining the corrosion current density by measuring the polarization curve. The analysis of the data (Figures 4–6 and Table 3) showed that the corrosion rate of the magnesium foils over time approaches 0.5 mm·year^{-1}, which is summarized in Table 4. The CR of 0.5 mm·year^{-1} relates to both results from tests in DMEM and in c-SBF. Comparison with other studies[8,14,32] showed that CR of 0.5 mm·year^{-1} is in a common range. The CR determined by electrochemical results appears higher. One important reason is that the polarization method cannot reflect the barrier effect of corrosion products on corrosion rates. Furthermore, the results correlate better in DMEM than in c-SBF. This means a rapid barrier effect due to oxides or carbonates can be observed in electrochemical testing, but a barrier that needs 4 days to be built up during immersion cannot be reflected by those measurements. Electrochemical results resemble more the initial stage of the surface. Considering that the electrochemical tests were performed at room temperature, even higher corrosion rates can be expected at 37°C. The determination of the corrosion rate in mm·year^{-1} is the conventional method according to ASTM G31-72. However, volume loss might be a better approach for thin degrading foils.

4.2 | Corrosion tests

Considering the CR results, the immersion tests in DMEM appeared to be the most reliable method. The pH stabilization during testing was possible, which is the base to carry out such in vitro tests. DMEM was chosen as an electrolyte because the composition and buffering system show a high similarity to blood plasma and the human pH regulation.[15] To receive reliable results using cell medium DMEM, handling in conditions as sterile as possible was essential. The variation of CR determined by H_2 collection is partially caused by reading errors; the main reason, however, appears to be the inhomogeneous oxide layer and carbon contamination on the foil surface before corrosion test. The variation of CR received by micro-CT measurements was even higher. CT data could not precisely distinguish the growing layer thickness from the metal phase. Furthermore, CT did not detect any possible thin oxide layer, which already existed before immersion. A great disadvantage of CT data compared with H_2 data is that the data set of one sample can only be collected at the end of the corrosion test and not at several times during the test. Moreover, CT is more time-consuming and expensive than gas collection.

4.3 | Surface modification

CR measurements respectively volume loss values, which were a result of immersion tests in DMEM and c-SBF, show a variation in data from one foil to the other (Figure 4). The study of the foil surface before testing showed a variation of oxide and carbon composition from foil to foil (XPS study, Figure 3) and a variation of oxide distribution within the surface (Figure 2). Therefore, it is concluded that the variation in CR measurements is caused due to variation in the quality of the foil surface. Foil surfaces having an inhomogeneous oxide distribution may have a higher corrosion rate than more homogeneous foil surfaces. Furthermore, high carbon or oxide content may increase inhomogeneous surface layer growth. However, more foils have to be studied to draw a direct correlation between a high or low corrosion rate and a specific surface state. In addition, the grain size and shape may vary from foil to foil, and could also cause a variation in CR, which also needs to be addressed in future studies.

The degradation velocity during immersion was very quick at the beginning. These observations lead to the conclusion that besides the long-term corrosion rate, which can be adjusted by the alloy composition, the treatment of the

surface of magnesium membranes will be a key step for successful controlled application. Considering the greater relation of surface to volume and the fragile thin structures of foils, appropriate surface treatments will be a challenge.

The degradation products play an important role in the biocompatibility of the implant. On the one hand, it might be a risk if insoluble phosphates and carbonates arise. On the other hand, as it was indicated by the XRD studies, the formation of a bioactive layer may take place in parallel to degradation, which appears as an important property. The advantage of the good mechanical properties of magnesium materials, compared with resorbable polymers and collagen, has been already discussed in Section 1. Furthermore, this advantage is also evident by the comparison with bioactive ceramics and glasses, as those materials are known to bond to living bone and also show very limited mechanical properties.

ACKNOWLEDGMENTS

The authors gratefully thank Regensburg Center of Biomedical Engineering (RCBE) for the supply of lab consumables. Furthermore, they thank Regensburg Center of Biomedical Engineering (RCBE) for the micro-CT facility, and they acknowledge the support from the Deutsche Forschungsgemeinschaft (DFG) in frame of the program "Forschungsgeräte" (INST 102/11-1 FUGG). They also thank Hans-Peter Braeu for operating the SEM Leo 1455 VP (Figure 7).

CONFLICT OF INTERESTS

The authors declare that there are no conflict of interests.

DATA AVAILABILITY STATEMENT

The data that support the findings of this study are available from the corresponding author upon reasonable request.

ORCID

Helga Hornberger http://orcid.org/0000-0002-5797-4936

REFERENCES

[1] J. Caballé-Serrano, A. Munar-Frau, O. Ortiz-Puigpelat, D. Soto-Penaloza, M. Peñarrocha, F. Hernández-Alfaro, *J. Clin. Exp. Dent.* **2018**, *10*, e477.
[2] I. A. Rodriguez, G. S. Selders, A. E. Fetz, C. J. Gehrmann, S. H. Stein, J. A. Evensky, M. S. Green, G. L. Bowlin, *Mouth Teeth* **2018**, *2*, 1.
[3] M. Chiapasco, M. Zaniboni, *Clin. Oral Implants Res.* **2009**, *20*, 113.
[4] N. T. Kirkland, N. Birbilis, M. P. Staiger, *Acta Biomater.* **2012**, *8*, 925.
[5] J. Degner, F. Singer, L. Cordero, A. R. Boccaccini, S. Virtanen, *Appl. Surf. Sci.* **2013**, *282*, 264.
[6] L.-Y. Cui, Y. Hu, R.-C. Zeng, Y.-X. Yang, D.-D. Sun, S.-Q. Li, F. Zhang, E.-H. Han, *J. Mater. Sci. Technol.* **2017**, *33*, 971.
[7] M. Dahms, D. Hoeche, N. A. Agha, F. Feyerabend, R. Willumeit-Römer, *Mater. Corros.* **2018**, *69*, 191.
[8] E. P. S. Nidadavolu, F. Feyerabend, T. Ebel, R. Willumeit-Römer, M. Dahms, *Materials* **2016**, *9*, 627.
[9] M. Esmaily, J. E. Svensson, S. Fajardo, N. Birbilis, G. S. Frankel, S. Virtanen, R. Arrabal, S. Thomas, L. G. Johansson, *Prog. Mater. Sci.* **2017**, *89*, 92.
[10] X. Gu, Y. Zheng, Y. Cheng, S. Zhong, T. Xi, *Biomaterials* **2009**, *30*, 484.
[11] A. Yamamoto, S. Hiromoto, *Mater. Sci. Eng., C* **2009**, *29*, 1559.
[12] D. Tie, F. Feyerabend, N. Hort, R. Willumeit, D. Hoeche, *Adv. Eng. Mater.* **2010**, *12*, B699.
[13] Y. Xin, T. Hu, P. K. Chu, *J. Electrochem. Soc.* **2010**, *157*, C238.
[14] X. Li, X. Liu, S. Wu, K. W. K. Yeung, Y. Zheng, P. K. Chu, *Acta Biomater.* **2016**, *45*, 2.
[15] J. Gonzales, R. Q. Hou, E. P. S. Nidadavolu, R. Willumeit-Römer, F. Feyerabend, *Bioact. Mater.* **2018**, *3*, 174.
[16] A.-I. Bita, A. Semenescu, A. Antoniac, I. Antoniac, *Key Eng. Mater.* **2016**, *695*, 152.
[17] H. Kalb, A. Rzany, B. Hensel, *Corros. Sci.* **2012**, *57*, 122.
[18] H. Y. Tok, E. Hamzah, H. R. Bakhsheshi-Rad, *Mater. Sci. Forum* **2015**, *819*, 331.
[19] J. Fan, X. Qiu, X. Niu, Z. Tian, W. Sun, X. Liu, Y. Li, W. Li, J. Meng, *Mater. Sci. Eng., C* **2013**, *33*, 2345.
[20] A. C. Hänzi, I. Gerber, M. Schinhammer, J. F. Löffler, P. J. Uggowitzer, *Acta Biomater.* **2010**, *6*, 1824.
[21] X. Zhang, G. Yuan, L. Mao, J. Niu, W. Ding, *Mater. Lett.* **2012**, *66*, 209.
[22] T. Kokubo, H. Takadama, *Biomaterials* **2006**, *27*(15), 2907.
[23] G. Song, A. Atrens, D. St John, in *Magnesium Technology 2001* (Ed: J. N. Hryn, Warrendale, Pennsylvania: The Minerals, Metals & Materials Society [TMS]) **2001**, *8*, 254.
[24] W.-D. Mueller, H. Hornberger, *Int. J. Mol. Sci.* **2014**, *15*, 11456.
[25] Y. Xin, T. Hu, P. K. Chu, *Acta Biomater.* **2011**, *7*, 1452.
[26] A. Atrens, M. Liu, N. I. Z. Abidin, *Mater. Sci. Eng., B* **2011**, *176*, 1609.
[27] H. Hornberger, F. Witte, N. Hort, W. D. Mueller, *Mater. Sci. Eng., B* **2011**, *176*, 1746.
[28] Y. Liu, D. Liu, C. You, M. Chen, *Front. Mater. Sci.* **2015**, *9*, 247.
[29] R. Willumeit, J. Fischer, F. Feyerabend, N. Hort, U. Bismayer, S. Heidrich, B. Mihailova, *Acta Biomater.* **2011**, *7*, 2704.
[30] M. Santamaria, F. D. Quarto, S. Zanna, P. Marcus, *Electrochim. Acta* **2007**, *53*, 1314.
[31] H. Hornberger, B. Striegl, M. Trahanofsky, F. Kneissl, M. Kronseder, *Mater. Lett.: X* **2019**, *2*, 100007.
[32] N. I. Z. Abidin, B. Rolfe, H. Owen, J. Malisano, D. Martin, J. Hofstetter, P. J. Uggowitzer, A. Atrens, *Corros. Sci.* **2013**, *75*, 354.

How to cite this article: H. Hornberger, H. Kissel, B. Striegl, M. Kronseder, F. Vollnhals, S. Christiansen. Bioactivity and corrosion behavior of magnesium barrier membranes. *Mater. Corros.* 2022;73:8–19. https://doi.org/10.1002/maco.202112385